

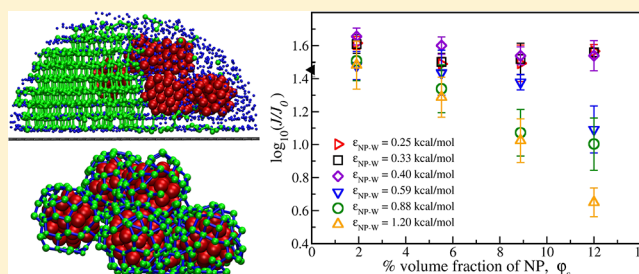
Ice Nucleation on a Graphite Surface in the Presence of Nanoparticles

Atanu K. Metya and Jayant K. Singh*¹

Department of Chemical Engineering, Indian Institute of Technology Kanpur, Kanpur 208016, India

Supporting Information

ABSTRACT: In this work, we have carried out a systematic study of nucleation of a supercooled nanofluid droplet on a graphite substrate using molecular dynamics simulations. In particular, the effect of nanoparticle (NP) loading (φ_s up to 12.0 vol %) in the supercooled liquid and the interaction strength between water and NP ($\epsilon_{\text{NP-W}}$) on the behavior of ice nucleation is investigated. At lower $\epsilon_{\text{NP-W}}$, the nucleation rate is indifferent, while at higher $\epsilon_{\text{NP-W}}$, the nucleation rate is found to reduce with the addition of nanoparticles. We found the maximum rate of ice nucleation is at $\varphi_s = 1.91\%$ and $\epsilon_{\text{NP-W}} = 0.40$ kcal/mol, which is approximately 45 times more than that seen in the bulk water. We present in detail the effect of nanoparticle and nanoparticle–water interactions on the structure and composition of ice. The results demonstrate that the number of ice-like water molecules in the nanofluid droplet decreases with increasing φ_s and $\epsilon_{\text{NP-W}}$, which correlates well with the lowering of the rate of ice nucleation at higher vol % of particle and stronger water–nanoparticle interaction. Therefore, the hydrophilicity of the nanoparticles inhibits nucleation. We further investigate the effect of the shape of nanoparticles on ice nucleation. The results suggest that the rate of ice nucleation is independent of particle shape of size ~ 1.2 nm. Finally, we try to draw a quantitative comparison with the water activity based ice nucleation theory.



INTRODUCTION

The formation of ice from supercooled water is of fundamental interest in both science and technology because it plays a central role in a wide variety of phenomena ranging from atmospheric processes to biological systems.^{1–3} It is well-known that heterogeneous nucleation processes occur in the presence of foreign particles or solid substrates.^{2,4} Atmospheric aerosol particles such as sea-salt, mineral dusts, volcanic dusts, or some organics generally play a vital role in the formation of ice particles in the atmosphere by different freezing modes.^{2,5–7} There are four basic modes of heterogeneous ice nucleation in which aerosol particles act as an ice nucleating particle: deposition nucleation, immersion freezing, condensation freezing, and contact freezing.⁸ Ansmann et al.⁹ suggested that the immersion freezing is of the most important freezing modes for ice nucleation processes in mixed phase clouds. In immersion freezing and contact freezing modes, the nucleation behavior depends on the molecular arrangement of water at the solid–liquid interface. Therefore, examining the relationship between nucleation behavior and solid–liquid interfacial structure is important for understanding the heterogeneous nucleation of ice. There are a number of studies on heterogeneous nucleation, which reports a range of nucleation behavior and the rate of ice nucleation in the presence of atmospheric particles.^{2,5,10–12} In addition, the condensable organic molecules present in the atmosphere can significantly affect the ice nucleation behavior.^{13,14} Furthermore, the nucleation ability or freezing efficiency of mineral dust strongly

depends on its type, size, and the amount present in the droplet.^{7,15–17}

The ability to tune the ice crystallization of supercooled liquid in the presence of nanometer-sized particles suspended in liquid (also known as nanofluids) is important for both naturally occurring and technological processes. Nanofluids are important due to their rapidly growing demand in numerous scientific and technological processes. These include areas such as cloud seeding, electronic and medical applications, and environmental chemistry.^{2,18–21} The use of suspended nanoparticles (NPs) as an additive to the base liquid can significantly modify the thermo-physical and transport properties such as thermal conductivity, boiling heat transfer coefficient, thermal diffusivity, and viscosity.^{20,22} The wetting behavior of nanofluids on the solid surfaces is of particular interest to various technological applications such as microfluidics and nanoprinting devices,^{23,24} where the surface tension of the nanofluids and the contact area between the solid substrate and the nanofluid play a vital role in these processes. The aforementioned applications are inherently dependent on the competitive NP–NP, fluid–fluid, NP–substrate, and NP–fluid interactions. Several theoretical and experimental studies have been conducted on the wettability of nanofluids on the solid surfaces.^{25–28} Wasan and Nikolov²⁶ reported the enhanced spreading dynamics of nanofluid in the

Received: June 23, 2018

Published: July 27, 2018

presence of nanometer-sized particles. Theoretical and experimental investigations have suggested that the nanoparticles near the three phase contact line form a solid-like ordering, as a result, the excess pressure at the contact line enhances the spreading of nanofluids.^{26–28} Recently, the wettability of a water nanodroplet containing nanoparticles on a solid surface has been studied using molecular dynamics (MD) simulation.²⁴ The results show that the addition of NPs to the base fluid inhibits the spreading kinetics of the nanofluid droplet, which is dependent on the fluid–particle interaction strength.²⁴

While there are a limited number of experimental studies of nucleation behavior of solutions or nanofluids on a solid surface, not many theoretical or molecular simulation studies are reported. Recently, Anim-Danso et al.²⁹ investigated the nucleation and freezing of salt solution on a solid surface using infrared–visible sum frequency generation spectroscopy (SFG). The results demonstrate that during cooling of salt solution, the brine solution is segregated near the solid surface, and finally, it forms salt-hydrate crystals next to the substrate.²⁹ Despite experimental observations,²⁹ molecular insight into the structure of the ice cluster at the solid–liquid interface remains poorly understood. Recently, molecular scale investigations with direct computational simulation^{25,30,31} have become a powerful tool to study the nucleation phenomena. There has been a growing body of computational works focused on heterogeneous ice nucleation of supercooled water in the presence of foreign particles or substrates.^{32–43}

Recently, equilibrium melting temperature and the kinetics of ice nucleation of supercooled nanodroplet as well as bulk water as a function of solute concentration have been studied using molecular dynamics simulations.^{32,44} It is known that the ice nucleation increases or decreases in the presence of various inorganic or organic species. For example, silver iodide, clay, and sand particles enhance the freezing point;⁴⁵ however, an addition of salts such as lithium, sodium, and potassium salts lower the freezing temperature of the supercooled water.⁴⁶ Zobrist et al.⁴⁷ studied the heterogeneous nucleation of various aqueous solutions in the presence of the different ice nuclei (nonadecanol, silica, silver iodide, and dust particles). The results showed that the freezing temperature reduces with increasing solute content in the solutions.⁴⁷ Thus, nanoparticle concentrations can play a significant role in the crystallization processes. However, the nucleation behavior in the presence of NPs at the molecular level, particularly near a substrate, is not well understood until date.

In this work, our aim is to elucidate the effect of nanoparticles, NP–water interactions, and the shape of the NP on ice crystallization of nanofluids. The role of the NPs is mainly to affect the droplet properties (i.e., colligative or water activity). Herein, we use the coarse-grained monatomic model of water (mW).⁴⁸ In this study, our aim is to elucidate the effect of nanoparticles, NP–water interactions, and the shape of the NP on ice crystallization of a supercooled droplet. Here, we evaluate the nucleation rate and explore the ice nucleation behavior as a function vol % of nanoparticle in the base fluid. Further, our interest is to provide molecular insights into ice structure at the solid–liquid interface.

MODEL AND SIMULATION DETAILS

The substrate is designed using two atomic layers of graphene (AB stacking) with an interlayer distance of 0.34 nm. The substrate is periodic in x - and y -directions with in-plane

dimensions of $\sim 3.41 \times 20.66 \text{ nm}^2$. The NPs are modeled as a face center cube (FCC) crystal of 0.408 nm lattice constant. Nanometer-sized particles are in spherical and cuboid shape where each NP contains 43 and 40 atoms, respectively (see Figure 1A). The effective diameter of a spherical NP is ~ 1.32

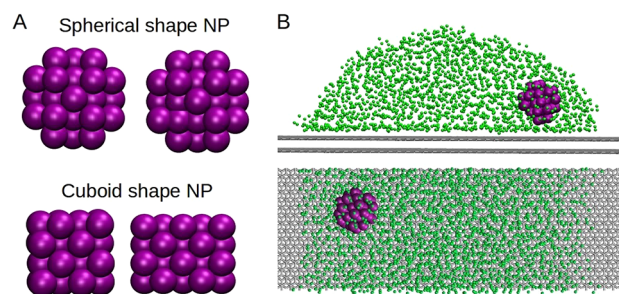


Figure 1. (A) Spherical (top) cuboid (bottom) shape of the nanoparticles. The purple balls represent atoms of a nanoparticle. (B) Representative cylindrical nanodroplet containing a nanoparticle on a smooth surface from both the top view (top) and side view (bottom) of a simulation system. The underlying graphite surfaces are shown in gray, while the small green balls represent the liquid water nanodroplet.

nm, whereas a cuboid NP with the dimensions of $\sim 1.109 \text{ nm} \times 0.905 \text{ nm} \times 0.905 \text{ nm}$. A typical cylindrical shape (length $l = 3.4 \text{ nm}$) of nanodroplet used in this study has 2000 water molecules as the base liquid. Figure 1B shows the representative snapshots (top and side views) of nanofluid droplet placed on a graphite substrate. The NP composition is represented in percentage volume fraction,

$$\varphi_s = \left(\frac{V_{\text{NP}}}{V_{\text{NP}} + V_{\text{W}}} \right) \times 100 \quad (1)$$

where V_{NP} and V_{W} are the volume of NP and water in the nanofluid, respectively. The volume of water and nanoparticles are calculated using the following equations:

$$\begin{aligned} V_{\text{W}} &= \nu N_{\text{W}} \\ V_{\text{NP}} &= \left(\frac{4}{3} \pi R^3 \right) N_{\text{NP}} \\ V_{\text{NP}} &= (L_x \times L_y \times L_z) N_{\text{NP}} \end{aligned} \quad (2)$$

where ν and N_{W} are the molecular volume of water in the mW model and number of water molecules, respectively. R is the radius of a spherical NP. L_x , L_y , and L_z are the length of a cuboid NP in x -, y -, and z -directions, respectively. In the present study, we have considered number of spherical nanoparticles $N_{\text{NP}} = 0, 1, 3, 5, \text{ and } 7$, corresponding to percentage volume fraction $\varphi_s = 0, 1.91, 5.52, 8.88, \text{ and } 12.00$, respectively, and number of cuboid NPs $N_{\text{NP}} = 0, 1, 3, 5, 7, \text{ and } 9$, corresponding to percentage volume fraction $\varphi_s = 0, 1.46, 4.27, 6.91, 9.42, \text{ and } 11.80$, respectively.

The coarse-grained model of water, the mW model, is used to describe the intermolecular interaction among the water molecules and is developed by Moore and Molinero⁴⁸ on the basis of the modified Stillinger–Weber (SW)⁴⁹ potential. The potential model is described using the functional form of the Stillinger–Weber (SW) potential, where the function includes two terms, a two-body term and a three-body term. The model exploits the structural similarity between water and the

tetrahedral semiconductors such as carbon, silicon, and germanium where the three-body term determines the strength of the local tetrahedral order. It was shown that in terms of tetrahedrality of an atom, water is located between carbon and silicon. By parametrization of two-body (the potential well depth and the equilibrium distance) and three-body (tetrahedral strength parameter) terms, the mW model reproduces the structure of water in liquid, glass, and ice states as well as many thermodynamic properties of ice.^{50–52} In particular, the mW model predicts that the melting temperature of ice Ih, 274.6 K, which is in good agreement with the experimental value (273.16).⁴⁸ Further, this model has shown that the cubic ice Ic is metastable as compared to the hexagonal ice Ih.⁵³ In the past few years, this model has been widely used to characterize the phase transitions and the structure of water under a variety of relevant environmental conditions.^{50,51,53–57} The interactions between substrate–water, substrate–NP, and NP–NP are modeled by the two-body term of the Stillinger–Weber (SW) potential. The water–carbon interaction parameters are adopted from the model of Lupi et al.,³⁴ which reproduces the macroscopic contact angle value of water on the graphite substrate surface. The NP–NP interaction is modeled by gold like interaction.⁵⁸ We have studied the effect of NP–water interactions by varying the interaction parameter ($\epsilon_{\text{NP-W}}$) in the range 0.25–1.20 kcal/mol (with a fixed value of $\sigma_{\text{NP-W}} = 0.305$ nm). The NP–substrate interaction parameters are $\sigma_{\text{NP-S}} = 0.32$ nm and $\epsilon_{\text{NP-S}} = 0.05$ kcal/mol. A standard SW cutoff of 1.8σ is considered.

The simulations are performed using the LAMMPS simulation package⁵⁹ under the canonical ensemble (constant number, volume, and temperature). The velocity-Verlet algorithm is used for integrating the equations of motion of water molecules with a time step of 10 fs in all the simulations. In the canonical ensemble, the temperature is controlled by a Nosé–Hoover thermostat with a relaxation time of 1.0 ps. Periodic boundary conditions are applied in the x - and y -directions, while the z -direction is nonperiodic and bounded with a reflective wall with sufficiently large space in order to avoid unnecessary interaction between a water droplet and a wall. The graphite substrate surface atoms are kept fixed during the simulations. The cylindrical water droplet on graphite substrate is initially equilibrated for 80 ns at a temperature of 300 K. An additional 70 ns simulations are performed to collect a large number of independent trajectories (store the trajectories at 1 ns interval) from the equilibrated system at 300 K. Subsequently, these stored trajectories act as a different initial configuration for independent nucleation simulation runs. We set our simulation at a temperature of 215 K for the nucleation study, which is instantaneously quenched from 300 to 215 K, and allowed the system to crystallize. The trajectories are collected after every 1000 steps for estimating the nucleation rate. For evaluation of liquid water layering on the graphite substrate surface, we perform separate simulations at 10 K higher than the temperature kept for the nucleation simulations, i.e., 225 K. This allowed us to collect sufficient statistics in the liquid state, without the onset of nucleation, within 20 ns simulations run for all the systems.

In this study, the CHILL algorithm⁵³ of Moore et al. is used to identify ice-like molecules from supercooled water. This algorithm is based on a local bond orientational parameter with respect to its four closest neighbors using the method of spherical harmonics, which was first proposed by Steinhardt et al.⁶⁰ and has been applied efficiently in numerous nucleation

and crystallization studies.^{31,61,62} For the local orientation around each particle i , we define a $2l+1$ components of a complex vector $\mathbf{q}_l(i)$ that identifies the order of a particle with respect to its four nearest neighbors. For the four closest neighbors of a particle i , the m th component of $\mathbf{q}_l(i)$ is defined as

$$q_{lm}^{(i)} = \frac{1}{4} \sum_{j=1}^4 Y_{l,m}(\hat{r}_{ij}) \quad (3)$$

where $Y_{l,m}(\hat{r}_{ij})$ is spherical harmonic with a particular value of l and m varies from $-l$ to $+l$. The correlation $d_l^{(ij)}$ between the nearby neighboring particles i and j is expressed by the normalized dot product of $\mathbf{q}_l(i)$ vectors with the same l -value, i.e.

$$\begin{aligned} d_l(i,j) &= \frac{\mathbf{q}_l^{(i)} \cdot \mathbf{q}_l^{(j)}}{|\mathbf{q}_l^{(i)}| |\mathbf{q}_l^{(j)}|} \\ &= \frac{\sum_{m=-l}^l q_{lm}^{(i)} q_{lm}^{*(j)}}{\left(\sum_{m=-l}^l q_{lm}^{(i)} q_{lm}^{*(i)}\right)^{1/2} \left(\sum_{m=-l}^l q_{lm}^{(j)} q_{lm}^{*(j)}\right)^{1/2}} \quad (4) \end{aligned}$$

In simulations, $l = 3$ or 6 (i.e., the order parameters q_3 or q_6) are utilized effectively to identify the ice-like molecule from supercooled liquid.^{53,54,56,62} In this work, we have applied $l = 3$ to distinguish ice-like molecules. According to the CHILL algorithm, the water molecules are classified whether they have a local orientational order of cubic ice (I_c) or hexagonal ice (I_h). A more detailed description of the algorithm and discussion of the order parameters are presented in ref 53 as well as in our previous work.⁴¹

In order to evaluate the rate of ice nucleation (J) of a supercooled nanofluid droplet on a graphite substrate, we adopted the mean first-passage time (MFPT) method as proposed by Wedekind et al.⁶³ This method has been applied successfully in a number of nucleation studies,^{51,64} because of its inherent ability to directly provide the nucleation time, the size of the critical nuclei, and the location of the nucleation barrier by fitting the MFPT curve using the following expression:⁶³

$$\tau(n) = \frac{\tau_j}{2} \{1 + \text{erf}[(n - n^*)c]\} \quad (5)$$

where τ_j and n^* are the nucleation time and the size of the critical nuclei, respectively. Parameter c is a constant related to the Zeldovich factor, Z , as $c = Z\sqrt{\pi}$. The nucleation time $\tau(n)$ is obtained for each cluster size n by averaging time over several nucleation simulations. The nucleation rate J is estimated from the volume V of the water and the time of nucleation τ_j , $J = 1/(\tau_j V)$. The volume of water (V) is evaluated from the molecular volume of ice (0.0306 nm³) in the mW model.⁵² The critical cluster size, n^* is obtained simply by fitting the MFPT using eq 5 (see Figure S1, Supporting Information). In the present study, we have used more than 50 independent successful nucleation simulations for the evaluation of the rate of ice nucleation.

RESULTS AND DISCUSSION

We first discuss the nucleation of ice from supercooled nanofluids on a graphite substrate with varying loading of NPs and NP–water interaction strengths. Figure 2 illustrates the snapshots of the nucleation and growth of ice along a typical

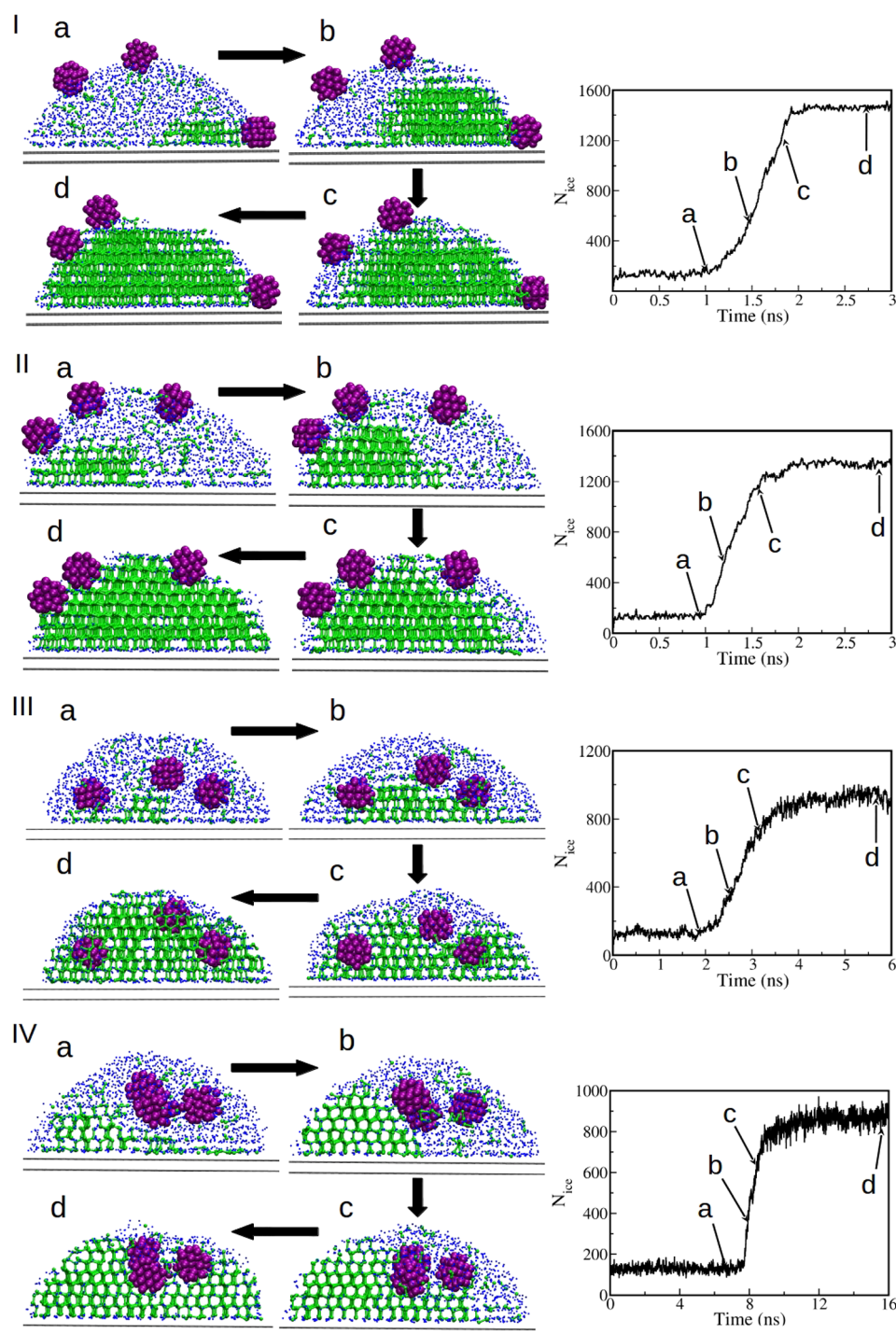


Figure 2. Isothermal crystallization of a nanofluid droplet on graphite surfaces at 215 K. Panels I–IV correspond to different nanoparticle–water interactions, $\epsilon_{NP-W} = 0.25, 0.40, 0.59, 0.88$ kcal/mol, respectively. Snapshots a–d show the different stages of cluster formation along a simulation of ice crystallization. Ice crystallites are represented as green balls and sticks, while liquid water molecules in the droplet are depicted by blue dots. The right panels show the number of ice-like molecules as a function of time and points a–d correspond to the snapshots of a simulation.

crystallization trajectory of a nanofluid drop at 215 K for the different NP–water interactions. Figure 2 (right panel) also displays the number of ice-like molecules as a function of time. Initially, small ice clusters are formed on the graphite substrate (see stage a), indicating a heterogeneous nucleation. Similar behavior has been observed for a pure water slab and droplet on a graphitic substrate.^{34,35,65} Stage a (the formation of ice cluster on the graphite substrate) is followed by a fast phase transition (stages b and c), and finally, it enters the growth

process. For lower values of ϵ_{NP-W} , all the nanoparticles reside at the vapor–liquid interface, as shown in Figure 2I,II. As ϵ_{NP-W} increases, the nanoparticles diffuse and stay inside the liquid droplets (see Figure 2III,IV). We have seen that the nucleation initiates at the substrate–liquid interface followed by the propagation of ice front. However, the NPs are mostly expelled from the crystallite and tend to form aggregates (see Figure S2). It should be noted that we do not find the nucleation of ice at particle–water interfaces, and nucleation is

initiated at the graphite surface for all the systems. This might be due to the size of the critical nucleus (22–30 water molecules), which is of the same order as that of a NP (size ~ 1.2 nm). In other words, the ratio of the radius of the NP to mean radius of the critical ice nucleus is ~ 1 . Thus, the effect of such small size of NPs is evident in the nucleation mechanism, which is seen to start from the substrate and the role of the NPs is mainly to affect the activity of water.

We next estimate the rate of ice nucleation of supercooled water in the presence of nanoparticles. In order to compare the heterogeneous nucleation rates of the nanofluids, the bulk nucleation rate calculated at the same temperature is used as a reference. The calculated nucleation rate of bulk water is $5.2 \pm 1.5 \times 10^{31} \text{ m}^{-3} \text{ s}^{-1}$ at 215 K using the MFPT method. Figure 3

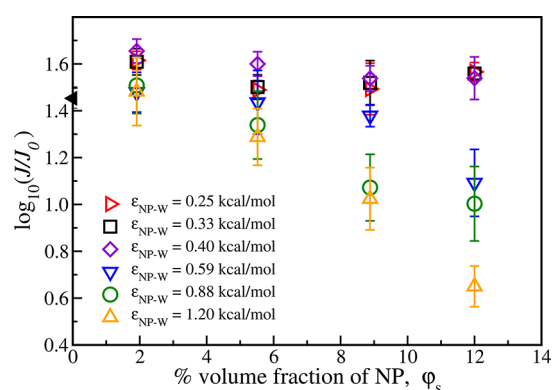


Figure 3. Nucleation rate as a function of percentage volume fraction of nanoparticles in the nanofluid at a temperature of 215 K for different nanoparticle–water interaction strengths. The values of the ice nucleation rate are expressed as $\log_{10}(J/J_0)$, where J_0 refers to the nucleation rate of bulk water at the same temperature. The black filled triangle symbol on the y -axis represents the rate in the absence of nanoparticle in a supercooled droplet. The error bars are the standard deviation of the block averages.

presents the nucleation rate as a function of percentage volume fraction of nanoparticle (i.e., loading of the nanoparticle) for different interaction strengths ($\epsilon_{\text{NP-W}}$) between the water molecules and the nanoparticles. At low vol % of NP, the effect of NP on nucleation behavior found to be indifferent to NP–water interaction strength. However, at a high volume fraction of NP significant variation in the nucleation rate is observed. The effect of loading of NP on ice nucleation is less for lower NP–water interactions ($\epsilon = 0.25, 0.33,$ and 0.40 kcal/mol) than for higher NP–water interactions ($\epsilon = 0.59, 0.88,$ and 1.2 kcal/mol).

At higher values of NP–water interactions ($\epsilon_{\text{NP-W}} = 0.59, 0.88,$ and 1.20 kcal/mol) the rate of ice nucleation reduces with increasing NP volume fraction. However, we have observed that at these NP–water interactions, the effect of the NP’s volume fraction on the nucleation behavior of the nanofluid is more pronounced at a higher volume fraction of NP than for a lower vol % of NP ($\phi_s = 1.91\%$) in the water. Interestingly, the nucleation rate is found to be highest at a NP–water interaction of 0.40 kcal/mol. We found that the maximum rate of ice nucleation in the presence of NPs is approximately 45 times higher at $\phi_s = 1.91\%$ than the value of bulk water. At higher nanoparticle content ($\phi_s = 12.00\%$), for $\epsilon_{\text{NP-W}} = 0.40$ and 1.20 kcal/mol the nucleation rate is approximately 32 and 5 times more than that of bulk water, respectively. On the basis of the behavior observed for different

volume fractions and interaction strengths, we can infer that at $\phi_s = 12.00\%$ or higher, the nucleation rate at $\epsilon_{\text{NP-W}} = 0.40$ kcal/mol is at least 6 times faster than that at $\epsilon_{\text{NP-W}} = 1.20$ kcal/mol. Recently, Cox et al.³⁷ investigated the heterogeneous ice nucleation of water in the presence of a hexagonal surface of a nanoparticle. The authors found that surface hydrophilicity can modify the ice nucleation and also observed a higher nucleation rate at an intermediate interaction strength. Our finding thus supports the work of Cox et al.³⁷ and confirms the enhanced nucleation rate at an optimal interaction strength between the NPs and water molecules in the nanofluids. We found that the critical ice nuclei appear at the top of the graphitic substrate. The size of the critical nucleus varies from 22 to 30 for different ϕ_s and $\epsilon_{\text{NP-W}}$ values considered in this work. This is in line with the previously reported range of the size of the critical nucleus in the literature, e.g., 10 and 50 at 205 K for crystallization of water on nanostructured⁶⁴ and smooth³⁸ substrates, respectively.

We now attempt to understand the aforementioned contrasting behaviors of the nucleation rate, which depends on the NP volume fraction as well as on the interaction strengths between the NPs and the water molecules. In order to know the mechanisms of ice crystallization, we have quantified different structures of the ice formed in the droplets. Here, we have evaluated the percentage of cubic ice, hexagonal ice, and interfacial ice (particle–liquid, substrate–liquid, and vapor–liquid interfaces) in the crystallized droplets. Figure 4 illustrates the compositions of ice-like and liquid-like molecules as a function of NP loading in the crystallized droplets for different NP–water interaction strengths. The composition of different types of ice appears to be independent with vol % of NP for $\epsilon = 0.25$ and 0.40 kcal/mol (see Figure 4a,b). The total of ice-like molecules at lower NP–water interaction strength is around 60–70% in the droplets. It is noted that at lower values of NP–water interactions ($\epsilon_{\text{NP-W}} \leq 0.40$ kcal/mol), the NPs stay at the vapor–liquid interface, as shown in Figure 5A(i–iii),B(i–iii). Consequently, the disruption of the six-member network structure of water molecules by the NPs is less. Thus, the ice-like molecules form a six-member network near the substrate, which promotes the ice crystallization. As the NP–water strength increases, the number of ice-like molecules reduced significantly with an increase in volume fraction of NPs (see Figure 4c,d). It is being reported experimentally by Maruyama et al.⁶⁶ that unfrozen water is present below the bulk freezing point. However, the amount of unfrozen water depends on the nature of substrate and interaction strength,⁶⁶ which is in line with our observation. At higher interaction strength, the composition of ice is affected by vol % of NP. In particular, the percentage of cubic and hexagonal ice decreases with an increase in the vol % of NP, while variations of the interfacial ice are found to be independent of NP loading. At these interactions, the fraction of unfrozen water increases with NP loading, while the ratio of cubic ice to hexagonal ice reduces with increase in the NP vol %. It indicates that some stacking disorder is present in the crystallite. The formation of disordered cubic and hexagonal stacking sequences with comparable fractions has been reported for the crystallization of water in bulk, nanopores, nanodroplets and aqueous droplets.^{52,53,55,67,68} This stacking disorder of ice appears to be more at higher vol % of NP. However, with increasing hydrophilicity of the NPs, the NPs stay inside the droplets (see Figure 5C(i–iii),D(i–iii)). Thus, the ice nucleation is hindered, and substantial stacking disorder ice is found mainly when the

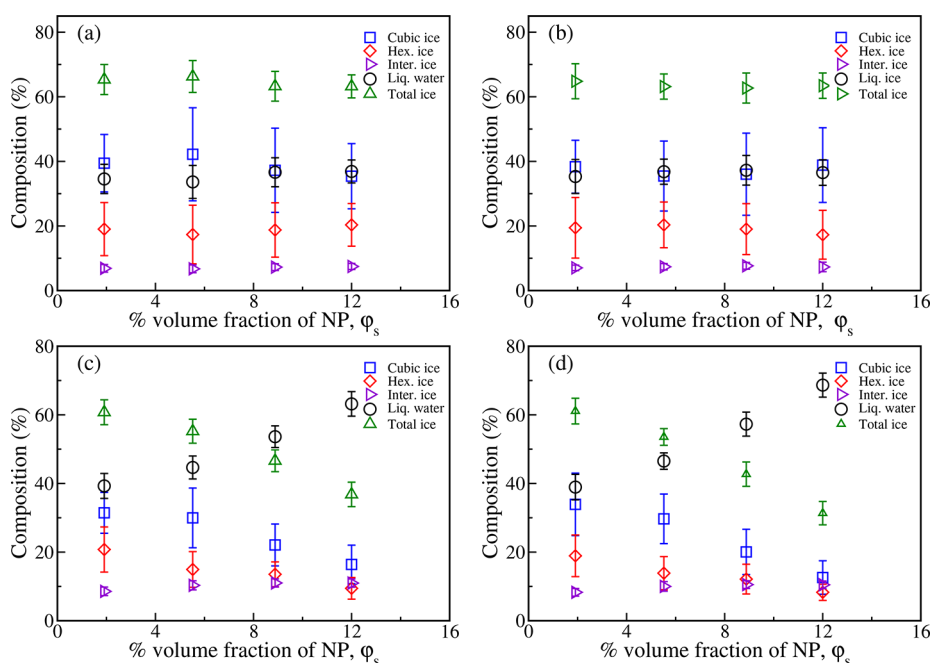


Figure 4. Percentage of cubic ice, hexagonal ice, interfacial ice, total ice-like, and liquid-like molecules as a function of percentage volume fraction of nanoparticles for different nanoparticle–water interactions. Panels a–d correspond to $\epsilon_{\text{NP-W}} = 0.25, 0.40, 0.59,$ and 0.88 kcal/mol, respectively. The error bars are the standard deviation of 30 nucleation simulations.

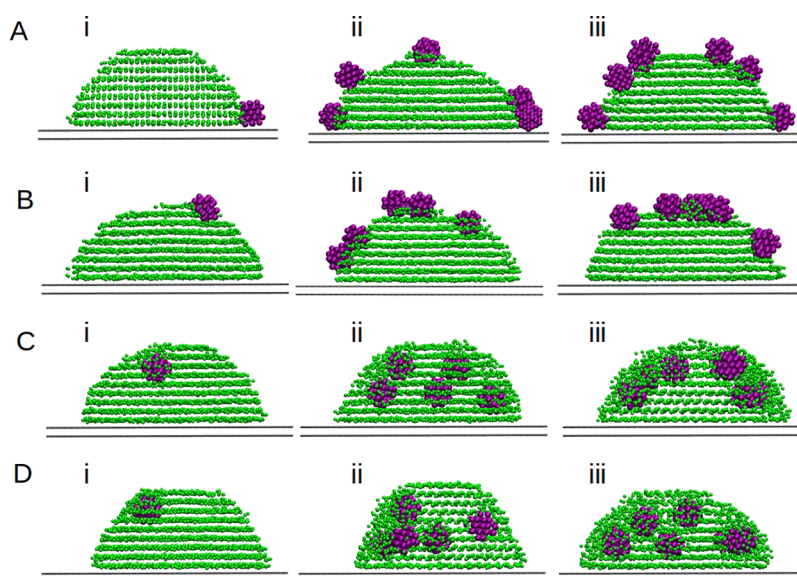


Figure 5. Representative snapshots of the crystallized nanodroplet of the nanofluids on solid surfaces. Panels A–D correspond to $\epsilon_{\text{NP-W}} = 0.25, 0.40, 0.59,$ and 0.88 kcal/mol, respectively. (Ai–Di, Aii–Dii, and Aiii–Diii) Snapshots of the corresponding system for $\phi_s = 1.91\%, 8.88\%$, and 12.00% , respectively.

NPs are present inside the droplets (i.e., for hydrophilic particles). As a consequence, a noticeable difference in the ice nucleation rate is found with increasing NP loading for higher NP–water strengths as compared to lower values of NP–water interaction.

Previous studies have reported that the layering of water at the solid surfaces correlates well with the heterogeneous nucleation of supercooled water.^{34,38,69} In order to address the effect of nanoparticle loading on the water layering at the graphite substrate, we perform separate simulations at 10 K higher than the temperature kept for the nucleation simulations (i.e., 215 K). This allowed us to collect sufficient

statistics in the liquid state, without the onset of nucleation, within 20 ns simulation runs for all the systems. Figure 6A represents the number density of water molecules as a function of distance in the direction perpendicular to the substrate for interaction strengths $\epsilon_{\text{NP-W}} = 0.25, 0.40, 0.59,$ and 0.88 kcal/mol. There are two major distinct peaks and two less intense peaks, which indicate the ordering of water molecules near the substrate. The peak height progressively decreases with the distance from the substrate, and around 1.5 nm away from the substrate, the density of water in the droplet approaches that of the bulk liquid. In order to quantify the degree of ordering of interfacial water in the presence of NPs, we have evaluated the

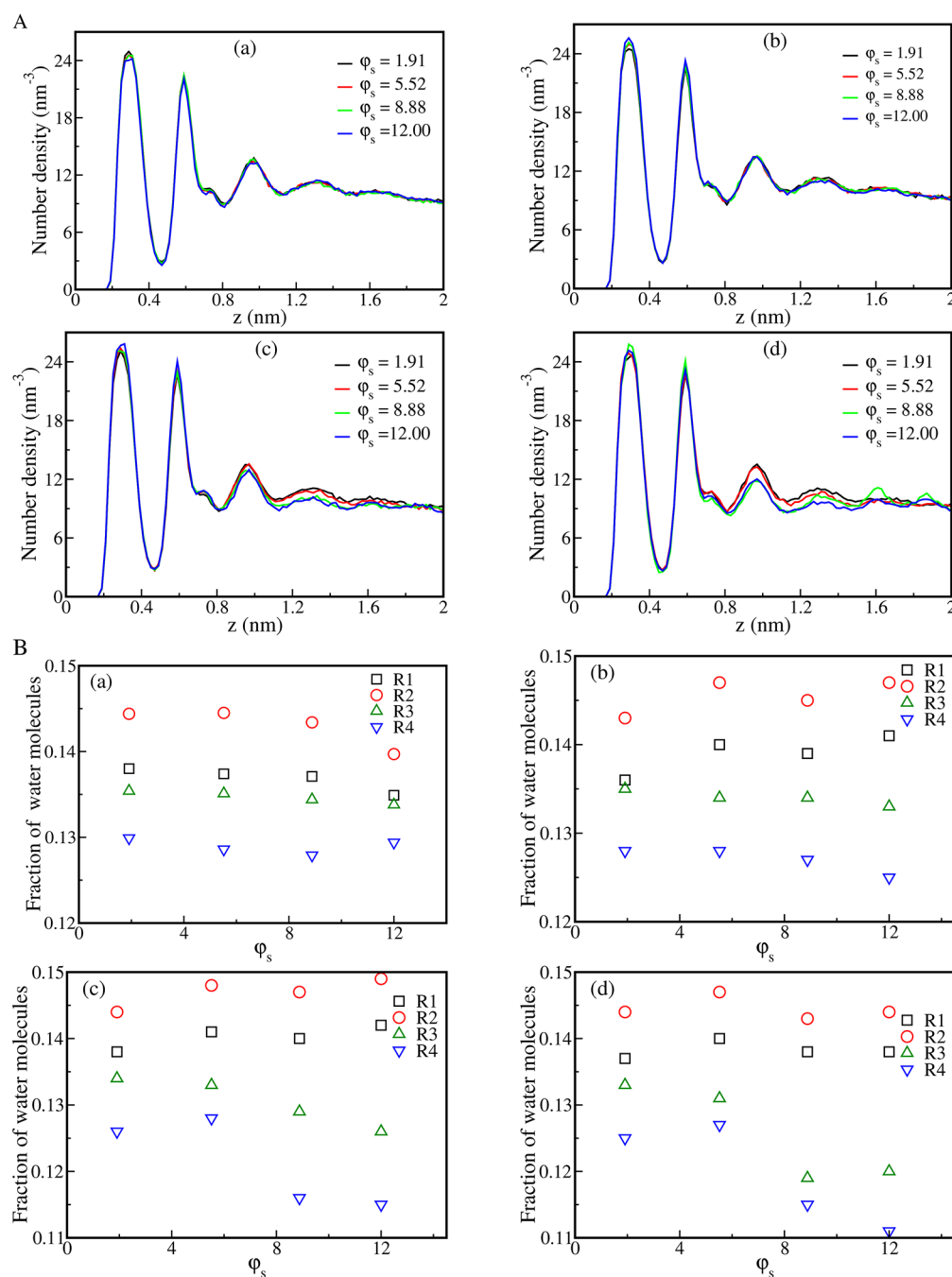


Figure 6. (A) Number density of liquid water in the nanofluids for various NPs loading at 225 K as a function of distance along the direction normal to the surface. Panels a–d correspond to $\epsilon_{\text{NP-W}} = 0.25, 0.40, 0.59,$ and 0.88 kcal/mol, respectively. (B) Fraction of water molecules in each layer as a function of the volume fraction of NPs in the nanodroplets. The layers 0.0–0.47, 0.47–0.81, 0.81–1.15, and 1.15–1.49 nm above the surface corresponds to R1, R2, R3, and R4, respectively.

fraction of water molecules present in different contact layers. Here we have considered four distinct regions, i.e., the distances 0.0–0.47, 0.47–0.81, 0.81–1.15, and 1.15–1.49 nm for first, second, third, and fourth layers, respectively. Figure 6B represents the fraction of water molecules in different layers close to the substrate as a function of volume fraction of NP in the nanofluids ($\phi_s = 1.91, 8.88,$ and 12.0%) for different NP–water interaction strengths ($\epsilon_{\text{NP-W}} = 0.25, 0.40, 0.59,$ and 0.88 kcal/mol). There is an insignificant variation in the fraction of water molecules close to the substrate (i.e., first and second layers) with an increase in NP concentration for all NP–water interaction strengths (see Figure 6B). At lower values of $\epsilon_{\text{NP-W}}$,

there is no significant variation of water molecules in the third and fourth layers because NPs reside at the vapor–liquid interface. However, as the NP–water interaction strength increases (cases for which NPs are present inside the water droplet), the effective number of water molecules in the third and fourth layers decrease with an increase in volume fraction of the NP in the nanofluids (see Figure 6B(c,d)), and as a consequence, the NPs inhibit nucleation of ice.

In order to further understand the structure of interfacial water near an NP surface, we analyze the number of ice-like and liquid molecules around an NP. Figure 7A presents the ice-like and liquid water molecules as a function of distance

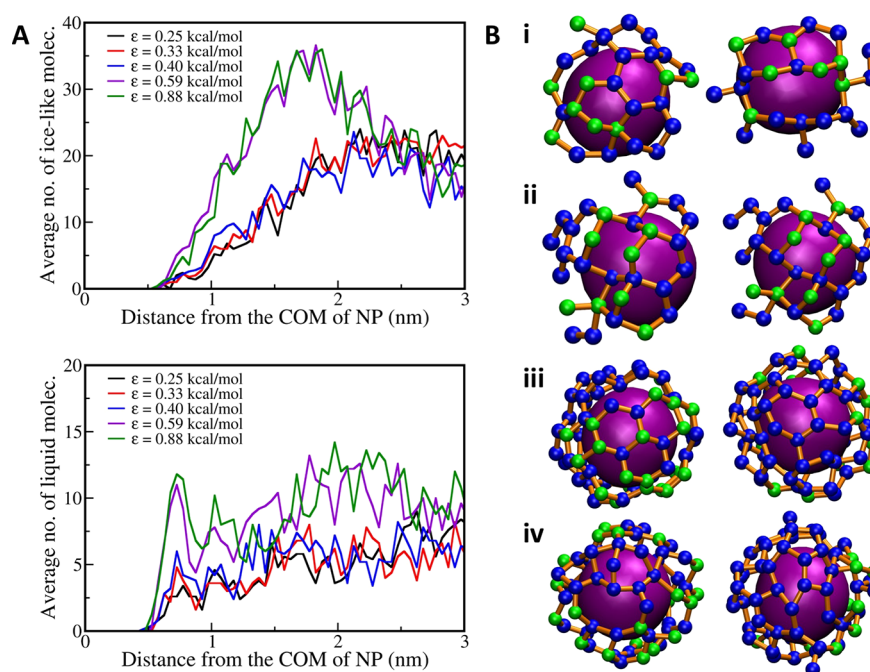


Figure 7. (A) Average number of ice-like and liquid water molecules as a function of distance from the center of mass of a NP with different NP–water interaction strengths for the volume fraction of NP, $\varphi_s = 1.91\%$, in the nanodroplet. (B) The structures of water molecules near to the nanoparticle surface at 215 K. The NP is shown as a big gray ball and the ice-like and water molecules in green and purple color balls. Panels i–iv correspond to $\epsilon_{NP-W} = 0.33, 0.40, 0.59,$ and 0.88 kcal/mol, respectively. Left and right columns represent the side views.

from the center of mass of an NP for $\varphi_s = 1.91\%$. With increasing NP–water interaction strengths, water molecules tend to adsorb on the surface of NP. Thus, the intensity of liquid-like water molecules enhances with increasing NP–water strengths (see Figure 7A (bottom)). Figure 7B displays the structure of the first water layer that forms on an NP surface for different ϵ_{NP-W} values (snapshots are randomly selected from nucleation trajectories). At low values of ϵ_{NP-W} , Figure 7B(i,ii) shows that the water molecules in the contact layer form mainly six-membered rings, with some presence of higher membered ring structures. However, at high values of ϵ_{NP-W} , water molecules form five- and six-membered networks, with a pronounced presence of the five-membered ring. This indicates that the implicit surface structure of NP is not commensurate with the underlying structure of the ice, which leads to inhibition of ice nucleation. Thus, at high values of ϵ_{NP-W} , the loading of NP plays a significant role in ice nucleation, and consequently, the nucleation rate of ice decreases with increasing φ_s .

As the size of the critical nucleus (using the molecular volume of ice) obtained in this study is of a size similar to that of the NP, the formation of ice embryo on such a small particle is negligible as per Fletcher,⁷⁰ which is in line with our observation. Therefore, the role of the NPs is mainly to affect the activity of water. Koop et al.^{71,72} introduced the water activity-based approach to describe homogeneous ice nucleation and to determine the freezing temperature and nucleation rate for pure water and the aqueous solution of various solutes. We have calculated the activity of water ($a_w = p_v/p_v^0$) in nanofluids at 298 K using grand canonical molecular dynamics simulations, following the procedure of Sirkin et al.⁷³ The detailed procedure for calculation of the water activity is included in the Supporting Information. The activity of water in nanofluids is found to be indifferent to NP loading for lower values of ϵ_{NP-W} , whereas the water activity decreases with an

increase in NP concentration (see inset Figure 8). The rate of ice nucleation reduces with the decrease in water activity, as

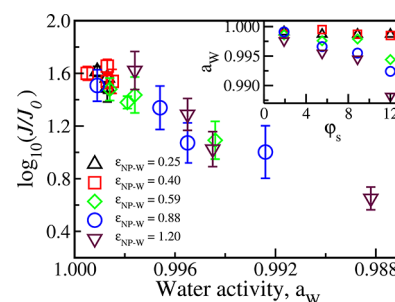


Figure 8. Nucleation rate as a function of water activity (a_w) in nanofluids at a temperature of 215 K. The activity of water in nanofluid is calculated at 298 K. The inset shows the activity of water as a function of the volume percentage of NP for the different interaction strengths between NP and water. The error in water activity is of less than 1%.

shown in Figure 8. At high values of NP–water interactions the rate decreases with an increase in NP loading, which is attributed to the lowering of the activity of water as clearly evident from Figure 8. Due to the higher interfacial interaction of water with NP, a lower amount of free water is available for crystallization at the graphite substrate. Thus, effectively, the NPs role is to reduce the water activity, particularly with increasing NP–water interaction. Therefore, our simulated results are consistent with the existing literature on the water–activity based ice nucleation theory.^{71,72,74}

Now, we turn our attention to study the effect of the shape of the NPs on the ice nucleation rate. It is well-known that geometry affects the surface to volume ratio, and thus it may affect the ice nucleation. Figure 9 presents the nucleation rate

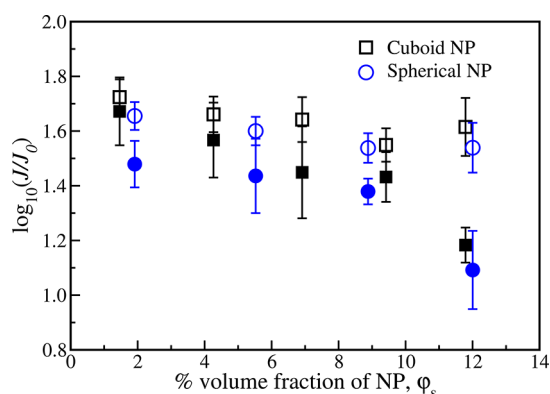


Figure 9. Variation of the nucleation rate with the percentage volume fraction of nanoparticles in the nanofluid at a temperature of 215 K. Open and filled symbols represent the NP–water interaction strength $\epsilon_{\text{NP-W}} = 0.40$ and 0.59 kcal/mol, respectively. The values of ice nucleation rate are expressed as $\log_{10}(J/J_0)$, where J_0 refers to the nucleation rate of bulk water at the same temperature. The error bars are the standard deviation of the block averages.

as a function of the volume fraction of NP for cuboid (square symbol) and spherical (circle symbol) shapes of the NP and different NP–water interaction strengths ($\epsilon_{\text{NP-W}} = 0.40$ (open symbol) and 0.59 (filled symbol) kcal/mol). For these small sizes of nanoparticles, we found that the rate of nucleation is independent of particle shape, considering large fluctuation and overlap of the error bars. Thus, on the basis of the extensive molecular dynamics simulations, we expect that control over ice nucleation might be achieved by varying the NP content and water–NP interaction. Further, we believe that the present work can help in understanding processes related to condensation and crystallization of water in the presence of natural or model aerosol particles.

CONCLUSIONS

Herein, we report the tuning of nucleation behavior through systematic analysis of both the volume fraction of NP in the base fluids and NP–water interaction strength, which is achieved via increasing the number of NP in the base fluids and varying NP–water interaction strengths using molecular dynamics simulations. Furthermore, we investigated the effect of geometry of the NPs on ice crystallization of nanofluids. In the present study, the central results are evaluation of nucleation rate and internal structure of the nanodroplets. The present study provides the role of nanoparticle loading and the hydrophobicity/hydrophilicity of nanoparticle on the heterogeneous nucleation of ice. The results of our simulations suggest that the rate of the ice nucleation reduces with the increasing vol % of particles in the base fluid. We have seen that at higher NP–water interaction strength, the rate of ice nucleation of the nanofluid droplets decreases with increasing volume fraction of nanoparticle in the base fluid. We found that a maximum rate of ice nucleation is 45 times higher at $\phi_s = 1.91\%$ with a NP–water interaction of 0.40 kcal/mol than for the bulk water. On the basis of our simulation results, at 12.00% volume fraction of NP in the droplet, the rate in the presence of the hydrophobic NPs is at least 3 times faster than that with the hydrophilic NPs. We evaluate that at lower values of NP–water interactions ($\epsilon_{\text{NP-W}} \leq 0.40$ kcal/mol) total ice-like molecules are $60\text{--}70\%$ for all vol % of NP. However, this value reduced significantly with an increase in volume fraction

of NPs for the strong NP–water interactions. This indicates that the ice crystallization efficiency is reduced, if the interaction strength is high, because of the large number of molecules adsorbed on the nanoparticle surface. Therefore, this simulation study demonstrates that nanoparticles may act as inhibitors with increasing vol % of NP when they are present inside water droplets. Thus, in principle, the presence of different natures of particles with increasing volume fraction in the nanofluid might influence the rate of nucleation to a certain extent. Finally, we considered the effect of the shape of the NPs on ice crystallization. The results suggest that the nucleation rate is independent of particle shape of size ~ 1.2 nm.

This systematic analysis of heterogeneous nucleation opens a new platform for understanding and modulating ice nucleation with varying NP–water interactions and particle loading. Thus, the findings of our present study is of significance for many fields of science and engineering—from the interactions of liquid drops in complex fluids to the nucleation of nanofluids or salt solutions on the substrates—as well as for applications such as cloud seeding, cryopreservation of cells, and the survival of living cells.^{2,7,5,76}

ASSOCIATED CONTENT

Supporting Information

The Supporting Information is available free of charge on the ACS Publications website at DOI: [10.1021/acs.jpcc.8b05989](https://doi.org/10.1021/acs.jpcc.8b05989).

The MFPT curve, water activity, and snapshot of the aggregation of Nps (PDF)

AUTHOR INFORMATION

Corresponding Author

*J. K. Singh. E-mail: jayantks@iitk.ac.in. Phone: 0512-259 6141. Fax: 0512-259 0104.

ORCID

Jayant K. Singh: 0000-0001-8056-2115

Notes

The authors declare no competing financial interest.

ACKNOWLEDGMENTS

This work is supported by the Department of Science and Technology (DST), Government of India. The computational resources are provided by the HPC cluster of the Computer Center (CC), Indian Institute of Technology Kanpur.

REFERENCES

- (1) Tabazadeh, A.; Djikaev, Y. S.; Reiss, H. Surface Crystallization of Supercooled Water in Clouds. *Proc. Natl. Acad. Sci. U. S. A.* **2002**, *99*, 15873–15878.
- (2) Murray, B. J.; O’Sullivan, D.; Atkinson, J. D.; Webb, M. E. Ice Nucleation by Particles Immersed in Supercooled Cloud Droplets. *Chem. Soc. Rev.* **2012**, *41*, 6519–6554.
- (3) Lintunen, A.; Hölttä, T.; Kulmala, K. Anatomical Regulation of Ice Nucleation and Cavitation Helps Trees to Survive Freezing and Drought Stress. *Sci. Rep.* **2013**, *3*, 2031.
- (4) Sear, R. P. The Non-Classical Nucleation of Crystals: Microscopic Mechanisms and Applications to Molecular Crystals, Ice and Calcium Carbonate. *Int. Mater. Rev.* **2012**, *57*, 328–356.
- (5) DeMott, P. J.; Hill, T. C. J.; McCluskey, C. S.; Prather, K. A.; Collins, D. B.; Sullivan, R. C.; Ruppel, M. J.; Mason, R. A. H.; Irish, V. E.; Lee, T.; et al. Sea Spray Aerosol as a Unique Source of Ice Nucleating Particles. *Proc. Natl. Acad. Sci. U. S. A.* **2016**, *113*, 5797–5803.

- (6) Alpert, P. A.; Aller, J. Y.; Knopf, D. A. Initiation of the Ice Phase by Marine Biogenic Surfaces in Supersaturated Gas and Supercooled Aqueous Phases. *Phys. Chem. Chem. Phys.* **2011**, *13*, 19882–19894.
- (7) Atkinson, J. D.; Murray, B. J.; Woodhouse, M. T.; Whale, T. F.; Baustian, K. J.; Carslaw, K. S.; Dobbie, S.; ÓSullivan, D.; Malkin, T. L. The Importance of Feldspar for Ice Nucleation by Mineral Dust in Mixed-phase Clouds. *Nature* **2013**, *498*, 355–358.
- (8) Pruppacher, H.; Klett, J. *Microphysics of Clouds and Precipitation*; Kluwer Academic Publishers: Dordrecht, 1997.
- (9) Ansmann, A.; Tesche, M.; Seifert, P.; Althausen, D.; Engelmann, R.; Fruntke, J.; Wandinger, U.; Mattis, I.; Müller, D. Evolution of the Ice Phase in Tropical Altocumulus: SAMUM Lidar Observations over Cape Verde. *J. Geophys. Res.* **2009**, *114*, D17208.
- (10) Spracklen, D. V.; Carslaw, K. S.; Merikanto, J.; Mann, G. W.; Reddington, C. L.; Pickering, S.; Ogren, J. A.; Andrews, E.; Baltensperger, U.; Weingartner, E.; et al. Explaining Global Surface Aerosol Number Concentrations in Terms of Primary Emissions and Particle Formation. *Atmos. Chem. Phys.* **2010**, *10*, 4775–4793.
- (11) Conen, F.; Morris, C. E.; Leifeld, J.; Yakutin, M. V.; Alewell, C. Biological Residues Define the Ice Nucleation Properties of Soil Dust. *Atmos. Chem. Phys.* **2011**, *11*, 9643–9648.
- (12) McGrath, M. J.; Olenius, T.; Ortega, I. K.; Loukonen, V.; Paasonen, P.; Kurtén, T.; Kulmala, M.; Vehkamäki, H. Atmospheric Cluster Dynamics Code: a Flexible Method for Solution of the Birth-death Equations. *Atmos. Chem. Phys.* **2012**, *12*, 2345–2355.
- (13) Kong, X.; Andersson, P. U.; Thomson, E. S.; Pettersson, J. B. C. Ice Formation via Deposition Mode Nucleation on Bare and Alcohol-Covered Graphite Surfaces. *J. Phys. Chem. C* **2012**, *116*, 8964–8974.
- (14) Papagiannakopoulos, P.; Kong, X.; Thomson, E. S.; Pettersson, J. B. C. Water Interactions with Acetic Acid Layers on Ice and Graphite. *J. Phys. Chem. B* **2014**, *118*, 13333–13340.
- (15) Lüönd, F.; Stetzer, O.; Welti, A.; Lohmann, U. Experimental Study on the Ice Nucleation Ability of Size-selected Kaolinite Particles in the Immersion Mode. *J. Geophys. Res.* **2010**, *115*, D14.
- (16) Pinti, V.; Marcolli, C.; Zobrist, B.; Hoyle, C. R.; Peter, T. Ice Nucleation Efficiency of Clay Minerals in the Immersion Mode. *Atmos. Chem. Phys.* **2012**, *12*, 5859–5878.
- (17) Broadley, S. L.; Murray, B. J.; Herbert, R. J.; Atkinson, J. D.; Dobbie, S.; Malkin, T. L.; Condliffe, E.; Neve, L. Immersion mode Heterogeneous Ice Nucleation by an Illite Rich Powder Representative of atmospheric Mineral Dust. *Atmos. Chem. Phys.* **2012**, *12*, 287–307.
- (18) Das, S. K.; Choi, S. U. S.; Patel, H. E. Heat Transfer in Nanofluids-A Review. *Heat Transfer Eng.* **2006**, *27*, 3–19.
- (19) Zhang, R.; Li, G.; Fan, J.; Wu, D. L.; Molina, M. J. Intensification of Pacific storm track linked to Asian pollution. *Proc. Natl. Acad. Sci. U. S. A.* **2007**, *104*, 5295–5299.
- (20) Trisaksri, V.; Wongwises, S. Critical Review of Heat Transfer Characteristics of Nanofluids. *Renewable Sustainable Energy Rev.* **2007**, *11*, 512–523.
- (21) Han, G.; Ghosh, P.; De, M.; Rotello, V. M. Drug and Gene Delivery using Gold Nanoparticles. *NanoBiotechnology* **2007**, *3*, 40–45.
- (22) Ahn, H. S.; Kim, M. H. A Review on Critical Heat Flux Enhancement With Nanofluids and Surface Modification. *J. Heat Transfer* **2011**, *134*, 024001.
- (23) Bonn, D.; Eggers, J.; Indekeu, J.; Meunier, J.; Rolley, E. Wetting and Spreading. *Rev. Mod. Phys.* **2009**, *81*, 739–805.
- (24) Lu, G.; Hu, H.; Duan, Y.; Sun, Y. Wetting Kinetics of Water Nano-Droplet Containing Non-Surfactant Nanoparticles: A Molecular Dynamics Study. *Appl. Phys. Lett.* **2013**, *103*, 253104.
- (25) Chu, X. L.; Nikolov, A. D.; Wasan, D. T. Monte Carlo Simulation of Inlayer Structure Formation in Thin Liquid Films. *Langmuir* **1994**, *10*, 4403–4408.
- (26) Wasan, D. T.; Nikolov, A. D. Spreading of Nanofluids on Solids. *Nature* **2003**, *423*, 156–159.
- (27) Kondiparty, K.; Nikolov, A.; Wu, S.; Wasan, D. Wetting and Spreading of Nanofluids on Solid Surfaces Driven by the Structural Disjoining Pressure: Statics Analysis and Experiments. *Langmuir* **2011**, *27*, 3324–3335.
- (28) Liu, K.-L.; Kondiparty, K.; Nikolov, A. D.; Wasan, D. Dynamic Spreading of Nanofluids on Solids Part II: Modeling. *Langmuir* **2012**, *28*, 16274–16284.
- (29) Anim-Danso, E.; Zhang, Y.; Dhinojwala, A. Freezing and Melting of Salt Hydrates Next to Solid Surfaces Probed by Infrared-Visible Sum Frequency Generation Spectroscopy. *J. Am. Chem. Soc.* **2013**, *135*, 8496–8499.
- (30) Auer, S.; Frenkel, D. Line Tension Controls Wall-Induced Crystal Nucleation in Hard-Sphere Colloids. *Phys. Rev. Lett.* **2003**, *91*, 015703.
- (31) Matsumoto, M.; Saito, S.; Ohmine, I. Molecular Dynamics Simulation of the Ice Nucleation and Growth Process Leading to Water Freezing. *Nature* **2002**, *416*, 409–413.
- (32) Hudait, A.; Molinero, V. Ice Crystallization in Ultrafine Water-Salt Aerosols: Nucleation, Ice-Solution Equilibrium, and Internal Structure. *J. Am. Chem. Soc.* **2014**, *136*, 8081–8093.
- (33) Singh, J. K.; Müller-Plathe, F. On the Characterization of Crystallization and Ice Adhesion on Smooth and Rough Surfaces using Molecular Dynamics. *Appl. Phys. Lett.* **2014**, *104*, 021603.
- (34) Lupi, L.; Hudait, A.; Molinero, V. Heterogeneous Nucleation of Ice on Carbon Surfaces. *J. Am. Chem. Soc.* **2014**, *136*, 3156–3164.
- (35) Lupi, L.; Molinero, V. Does Hydrophilicity of Carbon Particles Improve Their Ice Nucleation Ability? *J. Phys. Chem. A* **2014**, *118*, 7330–7337.
- (36) Lupi, L.; Kastelowitz, N.; Molinero, V. Vapor Deposition of Water on Graphitic Surfaces: Formation of Amorphous Ice, Bilayer Ice, Ice I, and Liquid Water. *J. Chem. Phys.* **2014**, *141*, 18C508.
- (37) Cox, S. J.; Kathmann, S. M.; Slater, B.; Michaelides, A. Molecular Simulations of Heterogeneous Ice Nucleation. I. Controlling Ice Nucleation Through Surface Hydrophilicity. *J. Chem. Phys.* **2015**, *142*, 184704.
- (38) Fitzner, M.; Sosso, G. C.; Cox, S. J.; Michaelides, A. The Many Faces of Heterogeneous Ice Nucleation: Interplay Between Surface Morphology and Hydrophobicity. *J. Am. Chem. Soc.* **2015**, *137*, 13658–13669.
- (39) Cabriolu, R.; Li, T. Ice Nucleation on Carbon Surface Supports the Classical Theory for Heterogeneous nucleation. *Phys. Rev. E* **2015**, *91*, 052402.
- (40) Bi, Y.; Cabriolu, R.; Li, T. Heterogeneous Ice Nucleation Controlled by the Coupling of Surface Crystallinity and Surface Hydrophilicity. *J. Phys. Chem. C* **2016**, *120*, 1507–1514.
- (41) Metya, A. K.; Singh, J. K.; Müller-Plathe, F. Ice Nucleation on Nanotextured Surfaces: The Influence of Surface fraction, Pillar Height and Wetting States. *Phys. Chem. Chem. Phys.* **2016**, *18*, 26796–26806.
- (42) Sosso, G. C.; Tribello, G. A.; Zen, A.; Pedevilla, P.; Michaelides, A. Ice Formation on Kaolinite: Insights from Molecular Dynamics Simulations. *J. Chem. Phys.* **2016**, *145*, 211927.
- (43) Qiu, Y.; Odendahl, N.; Hudait, A.; Mason, R.; Bertram, A. K.; Paesani, F.; DeMott, P. J.; Molinero, V. Ice Nucleation Efficiency of Hydroxylated Organic Surfaces Is Controlled by Their Structural Fluctuations and Mismatch to Ice. *J. Am. Chem. Soc.* **2017**, *139*, 3052–3064.
- (44) Bullock, G.; Molinero, V. Low-Density Liquid Water is the Mother of Ice: On the Relation Between Mesoscale Structure, Thermodynamics and Ice Crystallization in Solutions. *Faraday Discuss.* **2013**, *167*, 371–388.
- (45) Gokhale, N. R.; Spengler, J. D. Freezing of Freely Suspended, Supercooled Water Drops by Contact Nucleation. *J. Appl. Meteorol.* **1972**, *11*, 157–160.
- (46) Kanno, H.; Angell, C. A. Homogeneous Nucleation and Glass Formation in Aqueous Alkali Halide Solutions at High Pressures. *J. Phys. Chem.* **1977**, *81*, 2639–2643.
- (47) Zobrist, B.; Marcolli, C.; Peter, T.; Koop, T. Heterogeneous Ice Nucleation in Aqueous Solutions: the Role of Water Activity. *J. Phys. Chem. A* **2008**, *112*, 3965–3975.

- (48) Molinero, V.; Moore, E. B. Water Modeled As an Intermediate Element between Carbon and Silicon. *J. Phys. Chem. B* **2009**, *113*, 4008–4016.
- (49) Stillinger, F. H.; Weber, T. A. Computer Simulation of Local Order in Condensed Phases of Silicon. *Phys. Rev. B: Condens. Matter Mater. Phys.* **1985**, *31*, 5262–5271.
- (50) Moore, E. B.; Molinero, V. Ice Crystallization in Water's "No-Man's Land". *J. Chem. Phys.* **2010**, *132*, 244504.
- (51) Moore, E. B.; Molinero, V. Structural Transformation in Supercooled Water Controls the Crystallization Rate of Ice. *Nature* **2011**, *479*, 506–508.
- (52) Johnston, J. C.; Molinero, V. Crystallization, Melting, and Structure of Water Nanoparticles at Atmospherically Relevant Temperatures. *J. Am. Chem. Soc.* **2012**, *134*, 6650–6659.
- (53) Moore, E. B.; de la Llave, E.; Welke, K.; Scherlis, D. A.; Molinero, V. Freezing, Melting and Structure of Ice in a Hydrophilic Nanopore. *Phys. Chem. Chem. Phys.* **2010**, *12*, 4124–4134.
- (54) Li, T.; Donadio, D.; Russo, G.; Galli, G. Homogeneous Ice Nucleation from Supercooled Water. *Phys. Chem. Chem. Phys.* **2011**, *13*, 19807–19813.
- (55) Moore, E. B.; Molinero, V. Is it Cubic? Ice Crystallization from Deeply Supercooled Water. *Phys. Chem. Chem. Phys.* **2011**, *13*, 20008–20016.
- (56) Reinhardt, A.; Doye, J. P. K. Free Energy Landscapes for Homogeneous Nucleation of Ice for a Monatomic Water Model. *J. Chem. Phys.* **2012**, *136*, 054501.
- (57) Espinosa, J. R.; Sanz, E.; Valeriani, C.; Vega, C. Homogeneous Ice Nucleation Evaluated for Several Water Models. *J. Chem. Phys.* **2014**, *141*, 18C529.
- (58) Ghorai, P. K.; Glotzer, S. C. Molecular Dynamics Simulation Study of Self-Assembled Monolayers of Alkanethiol Surfactants on Spherical Gold Nanoparticles. *J. Phys. Chem. C* **2007**, *111*, 15857–15862.
- (59) Plimpton, S. Fast Parallel Algorithms for Short-Range Molecular Dynamics. *J. Comput. Phys.* **1995**, *117*, 1–19.
- (60) Steinhardt, P. J.; Nelson, D. R.; Ronchetti, M. Bond-Orientational Order in Liquids and Glasses. *Phys. Rev. B: Condens. Matter Mater. Phys.* **1983**, *28*, 784–805.
- (61) Radhakrishnan, R.; Trout, B. L. Nucleation of Hexagonal Ice (Ih) in Liquid Water. *J. Am. Chem. Soc.* **2003**, *125*, 7743–7747.
- (62) Auer, S.; Frenkel, D. Numerical Prediction of Absolute Crystallization Rates in Hard-Sphere Colloids. *J. Chem. Phys.* **2004**, *120*, 3015–3029.
- (63) Wedekind, J.; Strey, R.; Reguera, D. New Method to Analyze Simulations of Activated Processes. *J. Chem. Phys.* **2007**, *126*, 134103.
- (64) Zhang, X.-X.; Chen, M.; Fu, M. Impact of Surface Nanostructure on Ice Nucleation. *J. Chem. Phys.* **2014**, *141*, 124709.
- (65) Lupi, L.; Peters, B.; Molinero, V. Pre-ordering of Interfacial Water in the Pathway of Heterogeneous Ice Nucleation Does not Lead to a Two-Step Crystallization Mechanism. *J. Chem. Phys.* **2016**, *145*, 211910.
- (66) Maruyama, M.; Bienfait, M.; Dash, J.; Coddens, G. Interfacial Melting of Ice in Graphite and Talc Powders. *J. Cryst. Growth* **1992**, *118*, 33–40.
- (67) Kuhs, W. F.; Sippel, C.; Falenty, A.; Hansen, T. C. Extent and Relevance of Stacking Disorder in "Ice Ic. *Proc. Natl. Acad. Sci. U. S. A.* **2012**, *109*, 21259–21264.
- (68) Murray, B. J.; Knopf, D. A.; Bertram, A. K. The Formation of Cubic Ice under Conditions Relevant to Earth's Atmosphere. *Nature* **2005**, *434*, 202.
- (69) Cox, S. J.; Kathmann, S. M.; Slater, B.; Michaelides, A. Molecular Simulations of Heterogeneous Ice Nucleation. II. Peeling Back the Layers. *J. Chem. Phys.* **2015**, *142*, 184705.
- (70) Fletcher, N. H. Size Effect in Heterogeneous Nucleation. *J. Chem. Phys.* **1958**, *29*, 572–576.
- (71) Koop, T.; Luo, B.; Tsias, A.; Peter, T. Water Activity as the Determinant for Homogeneous Ice Nucleation in Aqueous Solutions. *Nature* **2000**, *406*, 611–614.
- (72) Koop, T.; Zobrist, B. Parameterizations for Ice Nucleation in Biological and Atmospheric Systems. *Phys. Chem. Chem. Phys.* **2009**, *11*, 10839–10850.
- (73) Perez Sirkin, Y. A.; Factorovich, M. H.; Molinero, V.; Scherlis, D. A. Vapor Pressure of Aqueous Solutions of Electrolytes Reproduced with Coarse-Grained Models without Electrostatics. *J. Chem. Theory Comput.* **2016**, *12*, 2942–2949.
- (74) Knopf, D. A.; Alpert, P. A. A Water Activity Based Model of Heterogeneous Ice Nucleation Kinetics for Freezing of Water and Aqueous Solution Droplets. *Faraday Discuss.* **2013**, *165*, 513–534.
- (75) Lee, R.; Warren, G.; Gusta, L. *Biological Ice Nucleation and its Applications*; APS Press, 1995.
- (76) Baker, M. B.; Peter, T. Small-Scale Cloud Processes and Climate. *Nature* **2008**, *451*, 299–300.